

Measurement of correlated b quark cross sections at CDF

The CDF Collaboration

Abstract

Using data collected during the 1992-1993 collider run at Fermilab, CDF has made measurements of correlated b quark cross sections where one b is detected from the lepton from semileptonic decay and the second b is detected with secondary vertex techniques. We report on measurements of the cross section as a function of the momentum of the second b and as a function of the azimuthal separation of the two b quarks, for transverse momentum of the initial b quark greater than 15 GeV. The vertex reconstruction techniques are valid over a large range in transverse momentum, starting at a minimum of 10 GeV. Results are compared to QCD predictions.

Contact Person: Dr. Paul F. Derwent
University of Michigan
E-Mail: derwent@fnald.fnal.gov

Studies of b production in $p\bar{p}$ collisions provide quantitative tests of perturbative QCD. For processes involving momentum transfers on the order of m_b , the strong coupling constant, α_s , becomes relatively small and perturbative methods are expected to work well. Measurements of inclusive cross sections for $p\bar{p} \rightarrow bX$ have been made at CDF [1] and UA1 [2]. Consideration of the process $p\bar{p} \rightarrow b\bar{b}X$ provides further opportunities for comparison of experiment and QCD calculations.

We will make measurements of correlated b quark cross sections, where one b is detected from the lepton from semileptonic decay and the second b is detected with secondary vertex techniques. We report on measurements of the cross section as a function of the transverse momentum of the second b ($d\sigma_b/dE_T$) and as a function of the azimuthal separation ($d\sigma/d\delta\phi$) of the two b quarks, for transverse momentum of the initial b quark greater than 15 GeV.

This paper presents the first correlated cross sections measured at CDF using a combination of lepton and vertex tags to identify b events. Starting with a well identified μ candidate, we look for the presence of a second b with secondary vertex techniques. Using jets with $E_T > 10$ GeV, we measure the cross section as a function of the \bar{b} transverse momentum and also the cross section as a function of the azimuthal angle between the b and \bar{b} quarks. For purposes of notation, we will consider the μ as coming from a b quark, and the jet as coming from a \bar{b} quark.

The CDF has been described in detail elsewhere [3]. The tracking systems used for this analysis are the silicon vertex detector (SVX), the central tracking chamber (CTC), and the muon system. The SVX and CTC are located in a 1.4 T solenoidal magnetic field. The SVX consists of 4 layers of silicon-strip detectors with $r - \phi$ readout, including pulse height information [4], with a total active length of 51 cm. The pitch between readout strips is 60 μm and a spatial resolution of 13 μm has been obtained. The first measurement plane is located 2.9 cm from the interaction point, leading to an impact parameter resolution of ≈ 15 μm for tracks with transverse momentum, p_t , greater than 5 GeV/c. The CTC is a cylindrical drift chamber containing 84 layers, which are grouped into alternating axial and stereo superlayers containing 12 and 6 wires respectively, covering the radial range from 28 cm to 132 cm. The central muon system consists of two detector elements. The Central Muon chambers (CMU), located behind ≈ 5 absorption lengths of material, provide muon identification over 85% of ϕ for the pseudorapidity range $|\eta| \leq 0.6$, where $\eta = -\ln[\tan(\theta/2)]$. This η region is further instrumented by the Central Muon Upgrade chambers (CMP), located after ≈ 8 absorption lengths. The calorimeter systems used for this analysis are the central and plug systems. The central subtends the range $|\eta| < 1.1$ and spans 2π in azimuthal coverage. The plug subtends the range $1.1 < |\eta| < 2.4$, again with 2π azimuthal coverage.

CDF uses a three-level trigger system. At Level 1, muon candidate events are selected with a trigger that requires the presence of a hit pattern, consistent with $p_t > 6$ GeV/c, in the CMU chambers and confirming hits in the CMP chambers. At Level 2, the trigger requires that the CMU chamber track match a track found in the CTC, using the Central Fast Track processor, with $p_t > 9.2$ GeV/c. At Level 3, the trigger requires a muon track in both the CMU and CMP chambers matched with a track found in the CTC, using the offline track reconstruction algorithm, with $p_t > 7.5$ GeV/c.

An inclusive muon sample is formed from the muon triggered sample with the following selection criteria: (1) reconstructed CTC track, $p_t > 9$ GeV/c, (2) muon tracks exist in both the CMU chambers and CMP chambers, (3) the χ^2 of the match between muon track and

the extrapolated CTC track match be less than 9 in the transverse view of both CMU and CMP chambers and be less than 12 for the longitudinal view in the CMU chambers, and (4) the track extrapolate and is found in the SVX fiducial region. There are 145784 events passing all requirements in this data sample.

Monte Carlo samples for b and c quarks are produced using ISAJET version 6.43 [5]. The CLEO Monte Carlo program [6] is used to model the decay of b hadrons. b quarks produced using the HERWIG Monte Carlo [7] are also used for systematic studies. One of the final state b partons is required to have $p_t > 15$ GeV. Events with a μ with $p_t > 8$ GeV are passed through the full CDF simulation and reconstruction package. The simulation used an average b lifetime of $c\tau = 420 \mu\text{m}$.

The μ acceptance and efficiency has three parts to it: (1) the fiducial acceptance for muons coming from b 's with $|\eta| < 1$, (2) the fraction of b 's, $p_t^b > p_t^{min}$, which decay to muons with $p_t > 9$ GeV and (3) the trigger and identification efficiencies for 9 GeV muons. The first two factors have been studied using the Monte Carlo samples described above. The trigger and identification efficiencies for muons are studied from the data, using J/ψ and Z^0 samples. All acceptance and efficiency numbers are summarized in table 1.

The p_t^{min} value is chosen according to the standard interpretation, where 90% of muons with $p_t > 9$ GeV come from b quarks with p_t greater than p_t^{min} . For this sample, the p_t^{min} value is 15 GeV, from studying a sample of b quarks generated with $p_t > 10$ GeV.

We find that $18.6 \pm 1\%$ of muons with $p_t > 9$ GeV pass through the CMU—CMP fiducial regions, where the error is statistical only. This value is for the entire η distribution of produced b quarks. Restricting the $|\eta|$ of the parent b quark to be less than 1, we find $39.2 \pm 2\%$ of muons with $p_t > 9$ GeV pass through the CMU—CMP chambers. From a study of b quarks with $p_t > 15$ GeV which decay to μ , we find that $10.7 \pm 0.1 \%$ (statistical error only) have $p_t > 9$ GeV. We use the branching ratio $B(b \rightarrow \mu) = 0.108 \pm 0.065$ which comes from direct measurements at CLEO [9]. This fraction includes the sequential decay contribution, which has been scaled by the relative branching ratios of $b \rightarrow \mu$ to $c \rightarrow \mu$. We have varied the mean $\langle z \rangle$ used in the b fragmentation [8] to study the effects in the geometric and kinematic acceptance. The systematic errors are therefore correlated. A 1σ variation in the mean $\langle z \rangle$ gives a $+1 - 6.5 \%$ change in the geometric acceptance and a $+9.7 - 10.8\%$ change in the kinematic acceptance.

The trigger efficiency is measured using independently triggered samples for each level of the system. The efficiency curves are then convoluted with the p_t spectrum of muons, to get the efficiency for a muon with $p_t > 9$ GeV. The combined efficiency of the L1, L2, and L3 triggers is measured to be 0.81 ± 0.024 . The efficiency of the muon reconstruction algorithms has been studied in detail in the muon plus charm meson cross section work [10] and is found to be 0.981 ± 0.003 . Given the presence of reconstructed stubs in the chambers, the matching efficiency has been studied in a J/ψ sample and found to be 0.987 ± 0.013 for the matching cuts used in this analysis. The requirement that the CTC track be in the SVX fiducial region, in combination with the SVX tracking efficiency, has an efficiency of 0.68 ± 0.021 .

The combined acceptance and efficiency for muons coming from b quarks with $p_t > 15$ GeV is $0.00239 +0.00030 - 0.00018$. This correction will be applied to all cross section numbers presented below. Therefore, there is a common uncertainty of $+12.4 - 7.5\%$ on all the cross sections coming from the μ acceptance and identification efficiency.

Geometric Acceptance	$0.392 +0.005 - 0.026$
Kinematic Acceptance	$0.107 +0.010 - 0.012$
Branching Ratio	0.108 ± 0.065
Trigger Efficiency	0.81 ± 0.024
Reconstruction Efficiency	0.981 ± 0.003
Matching Efficiency	0.987 ± 0.013
SVX requirement	0.68 ± 0.021
Combined Acceptance and Efficiency	$0.00239 +0.00030 - 0.00018$

Table 1: Summary of muon acceptance and efficiency numbers. The uncertainties in the kinematic and geometric acceptance are correlated.

For the correlated cross sections, we look for additional jets in the sample, binning by jet E_T and azimuthal opening angle. For each jet in the sample, we calculate a probability that the jet is consistent with coming from the primary vertex. Using input templates from b , c , and primary (light quark and gluon) jet Monte Carlo samples, we fit the data as a sum of these three processes. Assuming that the presence of the μ candidate signals an independent b quark, we can then make correlated cross section measurements. Correcting for the μ acceptance and identification requirements and the \bar{b} jet acceptance, and scaling by the integrated luminosity of the sample, we have differential cross section measurements.

We make use of a jet probability algorithm [11] which asks the question “Is the ensemble of tracks in this jet consistent with being from the primary vertex?” This algorithm compares track impact parameters to measured resolution functions in order to calculate for each jet a probability that it is attached to the origin. This probability is uniformly distributed for light quark or gluon jets, but is very low for jets with displaced vertices from heavy flavor decay. The algorithm assigns a probability between 0 and 1, where a probability value near 1 means the jet is very consistent with being primary, and a probability value near 0 means the jet is very inconsistent with being primary.

For jet clusters identified in the calorimeter, the algorithm selects a set of tracks, $p_t > 1$ GeV/ c , within a cone of 0.4 around the jet axis to be used in the calculation of the jet probability. There are loose cuts to affiliate the tracks with the primary vertex, in addition to track quality requirements [11]. We require that there be ≥ 2 tracks passing the quality requirements for the calculation of the probability.

Jets in this sample are required to have $E_T > 10$ GeV in a cone of radius 0.4, $|\eta| < 1.5$, have at least 2 good tracks, and be separated from the muon in $\eta - \phi$ space by $\Delta R \geq 1.0$. The cone of radius 1.0 was chosen so that the tracks clustered around the jet axis were separated from the μ direction. All jet energies in this paper are measured energies, not including corrections for known detector effects [12].

The \bar{b} jet acceptance combines the fiducial acceptance of the SVX and the CTC, the track reconstruction efficiency, and fragmentation effects. The simulation is used to calculate the combination of these pieces. The acceptance represents the fraction of b quarks which produce jets with $E_T > 10$ GeV, $|\eta| < 1.5$ and at least 2 good tracks inside a cone of 0.4

E_T Range	Acceptance
10 — 15	32.9 ± 1.9 %
15 — 20	46.3 ± 2.2 %
20 — 25	48.8 ± 2.9 %
25 — 30	50.8 ± 3.9 %
30 — 40	49.7 ± 4.2 %
40 — 50	49.8 ± 7.3 %

Table 2: \bar{b} jet acceptance as a function of jet E_T for $|\eta| < 1.5$ (statistical errors only).

$\delta\phi$ Range	Acceptance
0 — 22.5°	7.25 ± 2.2 %
22.5° — 45°	4.52 ± 2.0 %
45° — 67.5°	36.9 ± 3.0 %
67.5° — 90°	51.4 ± 0.8 %
90° — 112.5°	51.4 ± 0.8 %
112.5° — 135°	51.4 ± 0.8 %
135° — 157.5°	51.4 ± 0.8 %
157.5° — 180°	51.4 ± 0.8 %

Table 3: \bar{b} jet acceptance as a function of $\delta\phi$ of the two b quarks, for $E_T > 10$ and $|\eta| < 1.5$ (statistical errors only). The first three bins have lower acceptance due to the ΔR cut for identification of the two b jets.

around the jet axis, where there is also a b quark which decays to a μ with $p_t > 9$ GeV within the CMU-CMP acceptance. The \bar{b} jet acceptance is calculated separately as a function of the jet E_T and azimuthal opening angle between the two quarks.

The average acceptance for the \bar{b} is $\approx 40\%$. It ranges from $32.9 \pm 1.9\%$ (statistical error only) for $10 < E_T < 15$ GeV to $49.8 \pm 7.3\%$ for $40 < E_T < 50$ GeV. For $\delta\phi < 22.5^\circ$, the acceptance is $7.3 \pm 2.2\%$, while for $157.5^\circ < \delta\phi < 180^\circ$, the acceptance is $51.4 \pm 0.8\%$. Tables 2 and 3 show the bin by bin values used in the differential cross section measurements.

We have compared the values for the \bar{b} jet acceptance from ISAJET samples to the acceptance from HERWIG samples. The acceptance agrees within the statistical error in the samples as a function of E_T , differing at the 5% level. We will take this as an additional systematic uncertainty on the acceptance. In combination with a 10% uncertainty due to the vertex distribution for events in the SVX fiducial volume, we have a common 11.2% systematic uncertainty in all the jet acceptance numbers.

We use a binned maximum likelihood fit [13] to distinguish the b , c , and primary jet contributions in the sample. In this case, we use the results of the jet probability algorithm to define the variable that is used in the fit. We find that the $\log_{10}(\text{jet probability})$ shows stronger differentiation between b , c , and primary jets (see figure 1) than the jet probability

and will use this variable in the fitting algorithm. We fit over the range $-10 - 0$ in $\log_{10}(\text{jet probability})$, where the b , c , and primary contributions are constrained to be positive, but no other constraints are included in the fit. We use smoothed Monte Carlo distributions from b and c samples as the input shapes for heavy flavor to decrease the effects of limited Monte Carlo statistics. We model the primary jets with an exponential distribution, since a logarithm transforms a uniform distribution to an exponential distribution.

We have explored the effect of different Monte Carlo samples to form the input shape used in the fit. Using different input b Monte Carlo samples compared to a test distribution made with independent Monte Carlo samples shows a 5% change in the fit fractions. Changing the average b lifetime by 6% [14] changed the fit fraction by 3%. We include a 5.8% systematic uncertainty to our fit results to account for systematic errors in the fitting procedure and uncertainty of the b lifetime.

In figure 2, we show the distribution of $\log_{10}(\text{jet probability})$ for all jets in the μ sample, overlaid with the fit results. In this sample, the fit predicts 2620 ± 97 b jets, 2085 ± 180 c jets, and 13103 ± 161 primary jets for a total of 17808. There are 17810 events in the data sample. Figure 3 shows three comparisons of the data and fit results, showing the bin-by-bin difference in the results, the bin-by-bin difference divided by the errors, and the distribution of the difference divided by the errors. In these distributions, the errors are a combination of the statistical errors in the data points and the overall scale error in the fitted values. We do not include any error on the Monte Carlo shapes. From these distributions, we can see that the inputs model the data well. The difference divided by the errors has a mean of -0.04 and RMS of 1.08.

We have applied the fitting algorithm to several different samples of jets, where we have made different requirements on the transverse energy of the jet or the azimuthal separation between the μ and the jet. Applying the acceptance and efficiency numbers for the μ candidate, the \bar{b} jet acceptance and dividing by the integrated luminosity of the sample, we convert the number of fit \bar{b} jets into differential cross sections. All of the cross section numbers presented have a set of uncertainties in common. These come from the μ acceptance and identification (+12.4 - 7.5%), the fitting procedure (5.8%), the vertex acceptance (10%), the \bar{b} jet acceptance (5%), and the luminosity normalization (3.6%). The total common systematic error is +18.3 - 15.4%.

We look at the E_T distribution of the jet in the event, using 6 bins to cover the region between 10 GeV and 50 GeV in transverse energy. In each E_T bin, we do an independent fit of the $\log_{10}(\text{jet probability})$ distribution and then correct for the acceptance. Table 4 contains a summary of the number of \bar{b} jets, number of total jets, and the cross section in each E_T bin considered. Figure 4 shows the values of the cross section as a function of jet E_T for μ with > 9 GeV.

We also measure the cross section as a function of the azimuthal separation between the jet and the μ . The measured jet direction is a good measure of the initial \bar{b} direction, while the μ follows the b direction. We have chosen to use bins of 22.5° in $\delta\phi$, which is the width of the spread between the b direction and the μ direction. With this bin size, the azimuthal separation of the jet and μ is a good approximation of the azimuthal separation of the two quarks. Table 5 contains a summary of the number of jets, number of fitted \bar{b} jets, and the cross section in each $\delta\phi$ bin considered.

Figure 5 shows a comparison to a theoretical prediction, using the Mangano-Nason-Ridolfi

E_T range	Number of Jets	Number of fit \bar{b} jets	Cross Section (nb/GeV)
10 — 15	5695	650 ± 52	5.49 ± 0.63
15 — 20	4083	647 ± 48	3.88 ± 0.41
20 — 25	2680	452 ± 40	2.57 ± 0.32
25 — 30	1774	323 ± 33	1.77 ± 0.25
30 — 40	1915	308 ± 32	0.86 ± 0.13
40 — 50	835	145 ± 21	0.41 ± 0.085

Table 4: Cross section summary as a function of jet E_T . There is a common systematic uncertainty of +18.3 – 15.4% not included in the experimental points.

$\delta\phi$ Range	Number of Jets	Number of fit \bar{b} jets	Cross Section (nb/22.5°)
0 — 22.5°	83	11.7 ± 7.4	2.24 ± 1.58
22.5° — 45 °	143	35.8 ± 10.6	10.88 ± 5.78
45° — 67.5°	364	73 ± 16	2.25 ± 0.66
67.5° — 90°	442	81 ± 17	2.19 ± 0.48
90° — 112.5°	624	122 ± 20	3.30 ± 0.58
112.5° — 135°	1188	195 ± 27	5.27 ± 0.80
135° — 157.5°	3394	477 ± 43	12.9 ± 1.40
157.5° — 180°	11752	1624 ± 76	43.9 ± 3.34

Table 5: Cross section summary as a function of $\delta\phi$ between the jet and μ . There is a common systematic uncertainty of +18.3 – 15.4% not included in the experimental points.

calculation [15] with $m_b = 4.75$ GeV, MRSB structure functions, and $\mu^2 = m_b^2 + \langle p_t \rangle^2$ for $|\eta^b| < 1.$, $p_t^b > 15$ GeV, $|\eta^{\bar{b}}| < 1.5$, and $p_t^{\bar{b}} > 10$ GeV as input. We have smeared the parton p_t distribution with the expected energy scale and resolution of the CDF detector [16], and have normalized the $\delta\phi$ distribution to the cross section with smeared $p_t > 10$ GeV. The shapes of the theoretical prediction and the experimental data agree well, especially for $\delta\phi > 90^\circ$. Note that there is a large change in the acceptance for $\delta\phi < 60^\circ$ (see table 3) due to the ΔR separation requirement on the μ jet system.

In conclusion, we have presented the first measurements of correlated $b\bar{b}$ cross sections using a combination of lepton and vertexing techniques to identify the two b 's. We measure the differential transverse energy cross section for the \bar{b} , $d\sigma_{\bar{b}}/dE_T$, and the differential azimuthal cross section between the two quarks, $d\sigma/d\delta\phi$. The shape in the $\delta\phi$ distribution agrees well with theoretical predictions, but the overall normalization is roughly a factor of 1.3 higher than predicted.

We thank the Fermilab staff and the technical staffs of the participating institutions for their vital contributions. This work was supported by the U.S. Department of Energy and National Science Foundation; the Italian Istituto Nazionale di Fisica Nucleare; the Ministry of Education, Science and Culture of Japan; the Natural Sciences and Engineering Research Council of Canada; the National Science Council of the Republic of China; the A. P. Sloan Foundation; and the Alexander von Humboldt-Stiftung.

References

- [1] F. Abe, *et al.*, Phys. Rev. Lett. **71** 2396 (1993) and references therein.
- [2] C. Albajar, *et al.*, Phys. Lett. **B256** (1991).
- [3] F. Abe, *et al.*, Nucl. Inst. and Methods **A271** (1988) 387 and references therein.
- [4] Fermilab-Pub-94/024-E, submitted to Nucl. Inst. and Methods.
- [5] F. Paige and S.D. Protopopescu, BNL Report No. 38034, 1986 (unpublished).
- [6] P. Avery, K. Read, G. Trahern, Cornell Internal Note CSN-212, March 25, 1985, (unpublished).
- [7] G. Marchesini and B.R. Webber, Nucl. Phys. **B310**, (1988), 461;
G. Marchesini, *et al.*, Comput. Phys. Comm. **67** 465 (1992).
- [8] J. Chrin, Z. Phys. C **36**, 165 (1987).
- [9] S. Henderson, *et al.*, Phys. Rev. **D45**, 2212 (1992).
- [10] T. LeCompte, these proceedings, (GLS0092).
- [11] Fermilab-Pub-94/097-E, submitted to Phys. Rev. D.
- [12] F. Abe, *et al.*, Phys. Rev. **D45**, 1448 (1992);
F. Abe, *et al.*, Phys. Rev. **D47**, 4857 (1993).

- [13] F. Abe, *et al.*, Phys. Rev. Lett., 67, 2609 (1991).
- [14] In F. Abe, *et al.*, Phys. Rev. Lett. **71**, 3421 (1993), CDF presents an error of 5.8%.
- [15] M. Mangano, P. Nason, and G. Ridolfi, Nucl. Phys. **B373**, 295 (1992).
- [16] F. Abe, *et al.*, Phys. Rev. Lett., 70, 1376 (1993).

Figure 1: The $\log_{10}(\text{jet probability})$ distributions used as inputs to the fitting program. The b and c shapes are smoothed versions of Monte Carlo distributions, while the primary shape is an exponential function. The three distributions are normalized to equal area and shown on the same vertical scale.

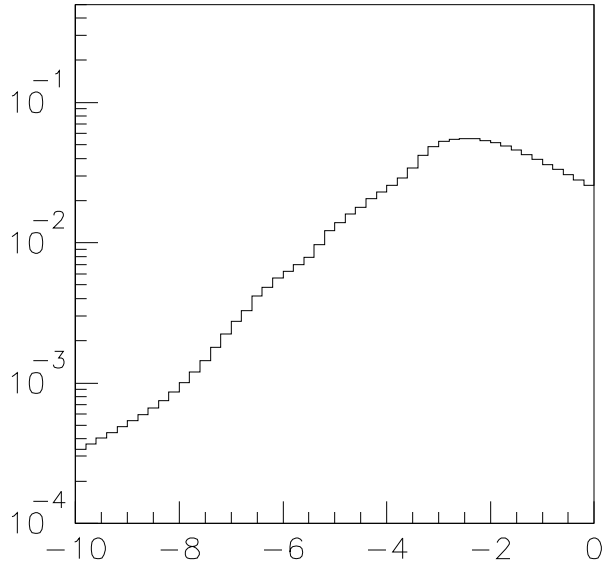
Figure 2: For 10 GeV jets in the μ sample, we show the data distribution overlaid with the fit results. Statistical errors on the data and scale errors on the fit results are included. The fit results model the data well over the entire range of the fit.

Figure 3: Various comparisons of the data distribution and the fit results. We show the bin by bin difference between the data and the fit results, the bin-by-bin difference scaled to the errors, and the distribution of the difference scaled to the errors. In all cases, the errors are the statistical error in the data points plus the overall scale error in the fitted values.

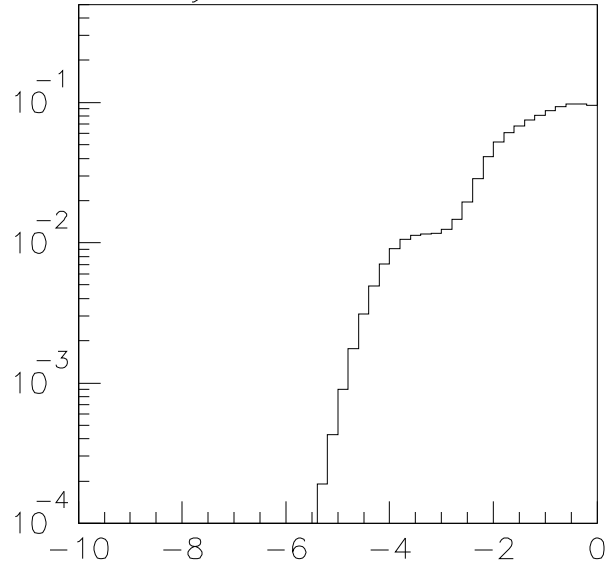
Figure 4: The distribution of the second b jet, $E_T > 10$ GeV and $|\eta| < 1.5$, cross section as a function of jet E_T , given a μ with $p_t > 9$ GeV present in the event. There is a common systematic uncertainty of $+18.3 - 15.4\%$ not included in the experimental points.

Figure 5: The distribution of the cross section as a function of the azimuthal angle between the μ and the jet, with $E_T > 10$ GeV and $|\eta| < 1.5$, overlaid with a theoretical prediction. The theoretical prediction has been normalized to the expected cross section after including the effects of detector smearing. There is a common systematic uncertainty of $+18.3 - 15.4\%$ not included in the experimental points. Note that the acceptance changes rapidly and has large uncertainty for the region $\delta\phi < 60^\circ$ due to the effects of the ΔR separation cut.

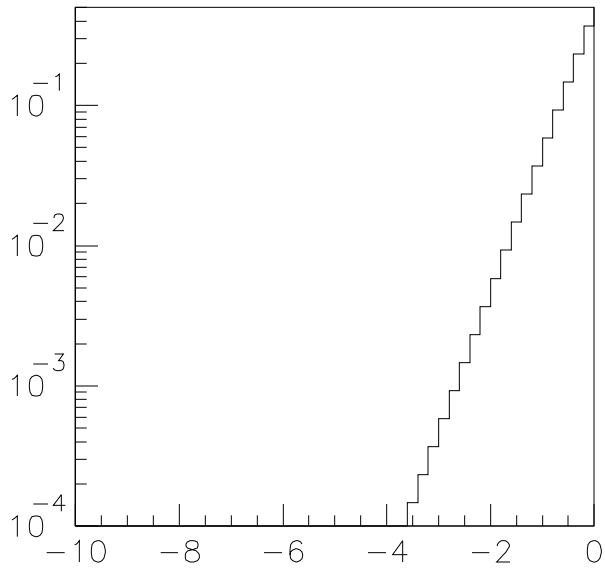
CDF Preliminary



b jet input distribution

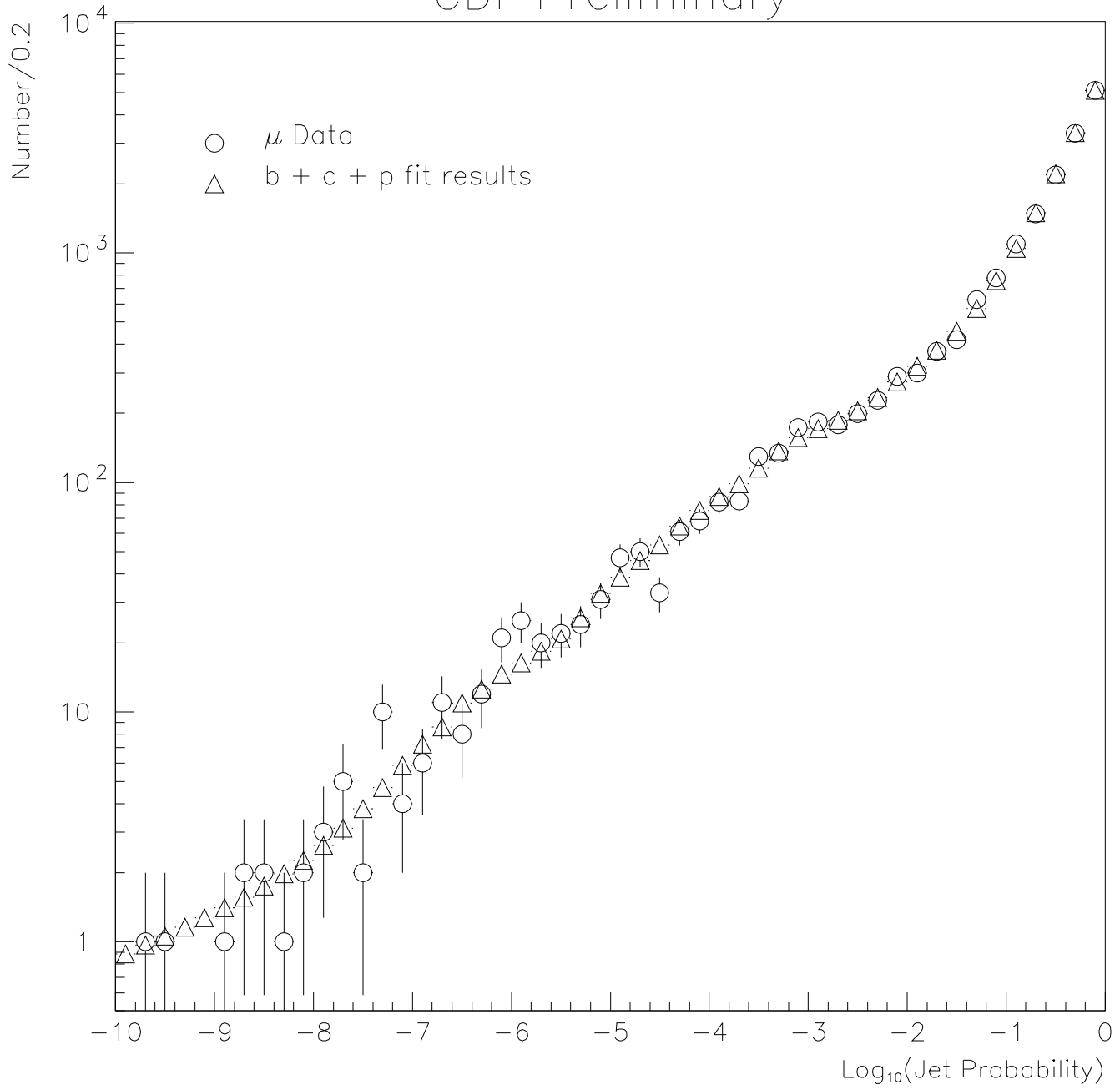


c jet input distribution

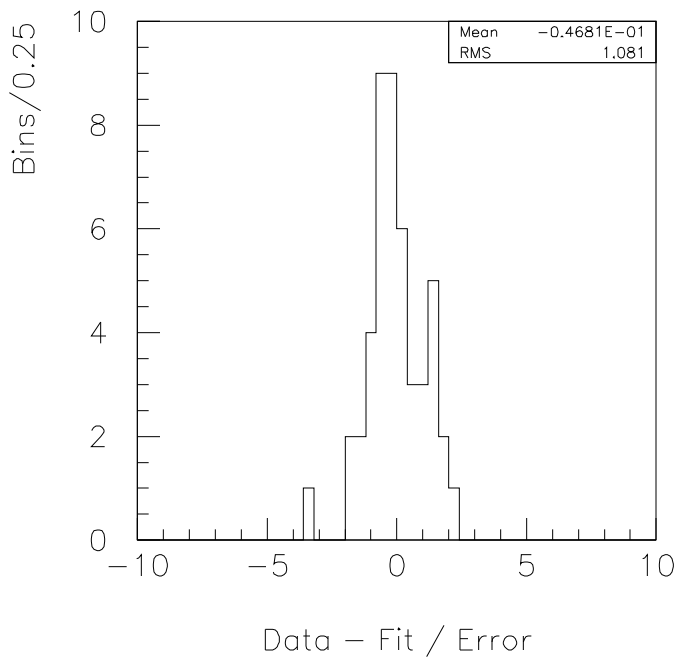
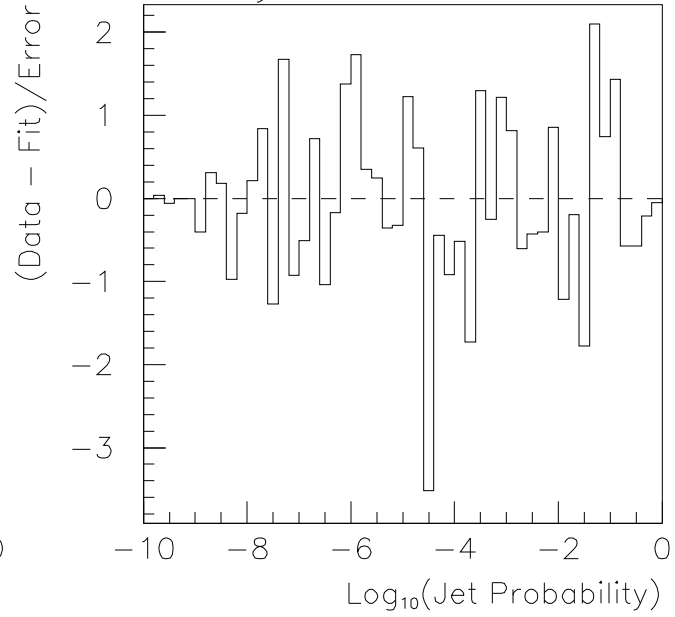
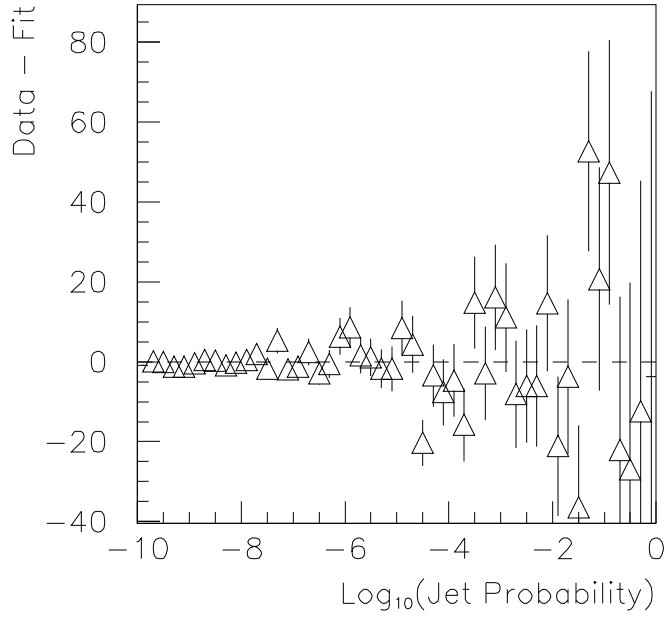


primary jet input distribution

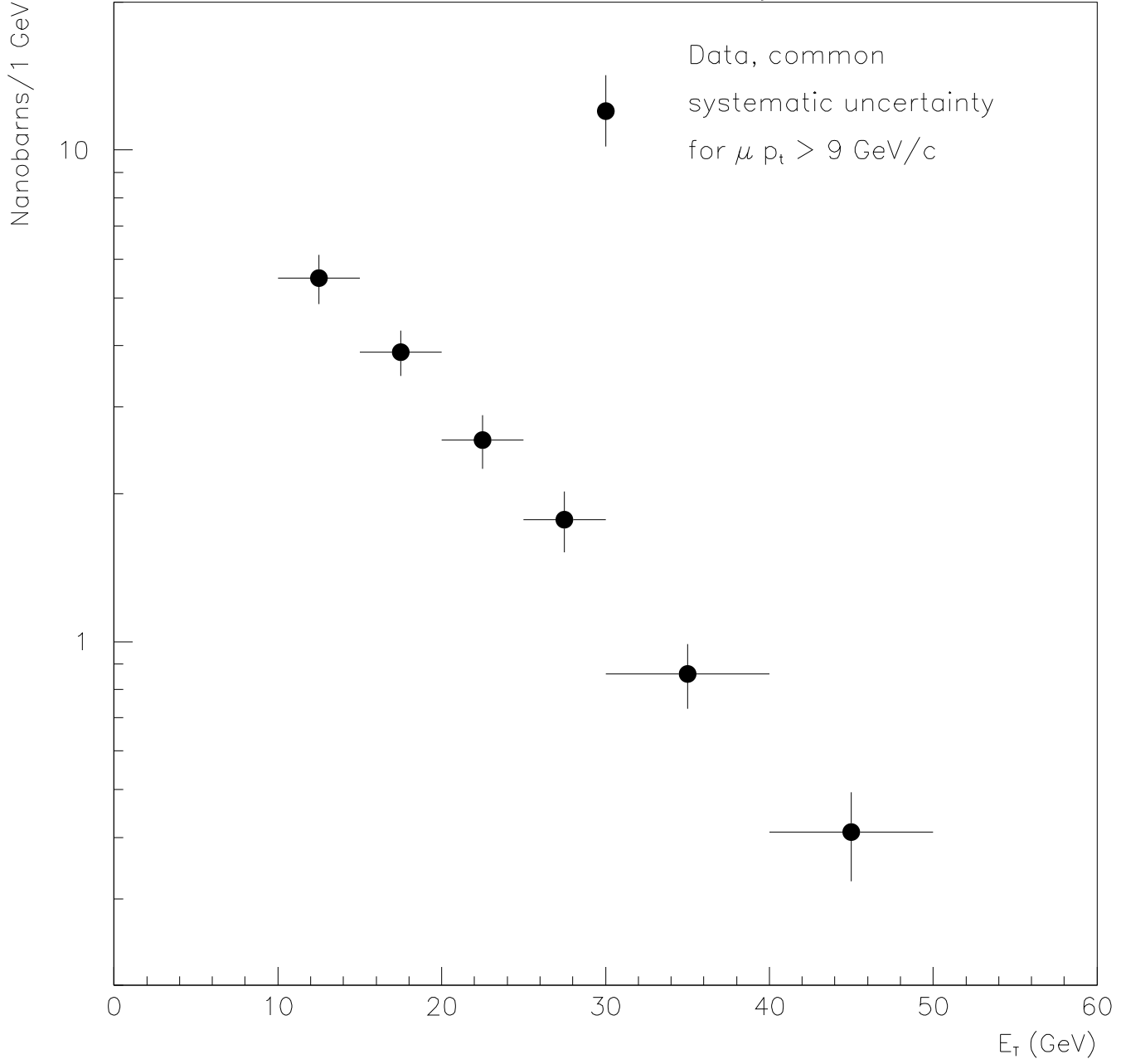
CDF Preliminary



CDF Preliminary



CDF Preliminary



CDF Preliminary

